Biochimica et Biophysica Acta 1838 (2014) 1247–1254

Contents lists available at ScienceDirect

Biochimica et Biophysica Acta

journal homepage: www.elsevier.com/locate/bbamem

Synthetic ion transporters: Pore formation in bilayers via coupled activity of non-spanning cobalt-cage amphiphiles

Lorale J. Lalgee [a], Lebert Grierson [a], Richard A. Fairman [a], Gina E. Jaggernauth [a], Albert Schulte [a,1], Roland Benz [b], Mathias Winterhalter [b,*]

[a] The Department of Chemistry, The University of the West Indies, St. Augustine, Trinidad and Tobago
[b] School of Engineering and Science, Jacobs University Bremen, Germany

ARTICLE INFO

Article history:
Received 24 August 2013
Received in revised form 7 January 2014
Accepted 27 January 2014
Available online 7 February 2014

Keywords:
Cobalt-cage metallosurfactant
Aza-crown spacer
Synthetic ion transporter
Lipid bilayer membrane
Liposomes

ABSTRACT

Three amphiphilic cobalt-cage congeners bearing a diaza-crown bridge and varying alkyl chains (**1**:**2**:**3**; n = 12, 16, 18) have been assessed for their ion transport across planar lipid bilayer membranes. In symmetrical electrolyte solutions, a range of ion transport activity is provoked: **1** disrupts painted (fluid) bilayers in a detergent-like mode of action; **2** forms conducting "pores" in folded (rigid) membranes with long open lifetimes (>2 min) while **3** requires the larger auxiliary solvent volume and lower lateral stress of painted membranes to effect ion transport via long-lived pores. Hill analysis of the conductance variation with monomer concentration yields coefficients (**2**:**3**; n = 2.3, 1.9) in support of dimeric (n = 2) membrane-active structures, for which the derived "pore" radii are correlated with charge-density of the transported cations and their affinity for the crown moiety. A toroidal-pore model is invoked to account for the flux of guest ions through planar bilayer membranes without a fast-diffusing intermediary or direct membrane-spanning structure.

1. Introduction

Natural ion channels constitute a large group of membrane proteins that allow the passive diffusion of ions across biomembranes. Their importance to the vitality of living organisms is evident in their ubiquity and their crucial role in physiological processes such as propagation of electrical signals in the nervous system, coordination of muscle contraction and transport in all tissues [1]. Consequently, the function of transmembrane ion channels is one of the most extensively studied areas in modern biological chemistry and validates a growing thrust to investigate synthetic systems capable of regulating ion flow across biological membranes. Current mimics of natural ion channels span an extensive array of structural archetypes [2–9] and transmembrane functional activity; from well-defined ion channels with ion-selectivity and gating properties [2–9] to membrane disrupting agents with non-specific activity [10]. These model systems not only contribute to our fundamental understanding of the behavior of naturally occurring ion channels, but are also pertinent to the development of non-natural antimicrobials [11], catalysts and sensors [12,13], as well as potential therapeutic agents [14].

Some common designs of synthetic ion transporters feature combinations of [2]: (a) a single [5] or self-assembled [7–9] membrane spanning moiety, (b) an embedded relay or selectivity region and (c) hydrophobic segments for membrane solubility and branching interactions with the membrane. Nevertheless, measured ion transport across bilayer membranes by synthetic carriers may be uncorrelated to these specifications, due to the diversity of kinetic, ionic, pseudophase aggregation behavior and interfacial phenomena that, in concert, defy practical trending of structure–activity relationships. We therefore aim to extend the range of available synthetic ion transporters which may usefully probe these variables by combining (1) an inert, yet highly charged head group, (2) a metal-coordinating midsection (guest cavity or ionophore) and (3) an aliphatic tail of variable chain length (Scheme 1).

Other groups have explored binary permutations of these factors, ranging from head groups with molecular recognition capability [15] to n-tailed metallo-surfactants [16,17] and geminis [2,18,19] (double-headed groups, bolaamphiphiles). However, the simplicity of components in our ternary molecular configuration affords control of (i) hydrophobicity; through chain length variation, (ii) strength of host–guest interactions; variable by macrocycle ring size and donor atoms, and (iii) headgroup charge-density; limited or enhanced by the amide linker between the ionophore and the highly-charged pendant cage. Such a "stacked functionality" surfactant is at once a well-defined probe for modeling interactions at the interface, bilayer membrane interior, and aqueous environments of surfactant-lipid assemblies where host–guest interactions engender molecular recognition and ion transport.

* Corresponding author at: Jacobs University Bremen, School of Engineering and Science, Research II, Campus Ring 1, 28759 Bremen, Germany. Tel.: +49 421 200 3248.
E-mail addresses: lorale.lalgee@sta.uwi.edu (L.J. Lalgee), Lebert.grierson@sta.uwi.edu (L. Grierson), Richard.fairman@sta.uwi.edu (R.A. Fairman), gina.jaggernauth@sta.uwi.edu (G.E. Jaggernauth), schulte@sut.ac.th (A. Schulte), r.benz@jacobs-university.de (R. Benz), m.winterhalter@jacobs-university.de (M. Winterhalter).
[1] Biochemistry–Electrochemistry Research Unit, School of Chemistry and Biochemistry, Institute of Science, Suranaree University of Technology, Thailand.

0005-2736/$ – see front matter © 2014 Elsevier B.V. All rights reserved.
http://dx.doi.org/10.1016/j.bbamem.2014.01.032

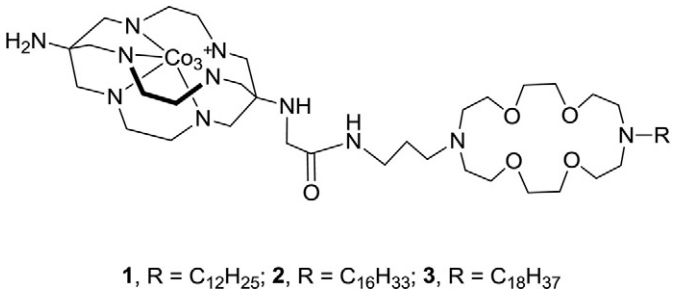

1, R = $C_{12}H_{25}$; **2**, R = $C_{16}H_{33}$; **3**, R = $C_{18}H_{37}$

Scheme 1. Structure of compounds **1**–**3** used in this study.

The large biological activity of amphiphiles such as **1**–**3** with the cobalt-cage headgroup [20–23] is attributed to two deterministic factors. The first is the electrostatic affinity of a negatively charged cell membrane for the highly charged cage, which ensures a high rate of membrane binding. Secondly, the embedded surfactants impose positive-curvature strain on the planar membrane [24,25] which is relieved by inward movement of the amphiphiles to maintain electrical neutrality. Ultimately, intracellular osmotic pressure increases and the cell ruptures. For supported bilayer membranes, a more detailed toroidal pore formulation is relevant. In this treatment the alien surfactant forces the membrane lipids to tilt relative to the bilayer normal, forming a well-defined, water-filled core that is lined by both alien and native lipid headgroups. Having a macrocyclic auxiliary, compounds **1**–**3** should enhance solubilization of guest ions in the bilayer, resulting in high rates of transmembrane ion flux. In related studies of **1** [26], a dramatic increase in the effective mean molecular area of the headgroup occurred with Mg^{2+} ions, indicative of high selectivity by the crown and also that changes in orientation of the molecule at the interfacial region are triggered by coordination of the guest. We apply the voltage clamp technique [1,27] in this work to directly assess the ion transport properties of **1**–**3** in the presence of different cations in the aqueous phase.

Given the new combined features of **1**–**3**, whether their aqueous aggregation behavior conforms to the standard packing parameter model (PPM) [28] is intriguing. According to the PPM, the nature of aggregate structures in water depends on hard-sphere type repulsive interactions of the head group (a = area), its size relative to the tail (l = length) and the total solvated volume of the amphiphile, V, through p = V/al. Limiting values of p are strongly correlated with aggregates shaped as spheres (<1/3) or cylinders (<1/2), vesicles(<1) planar lamellae (≈1)

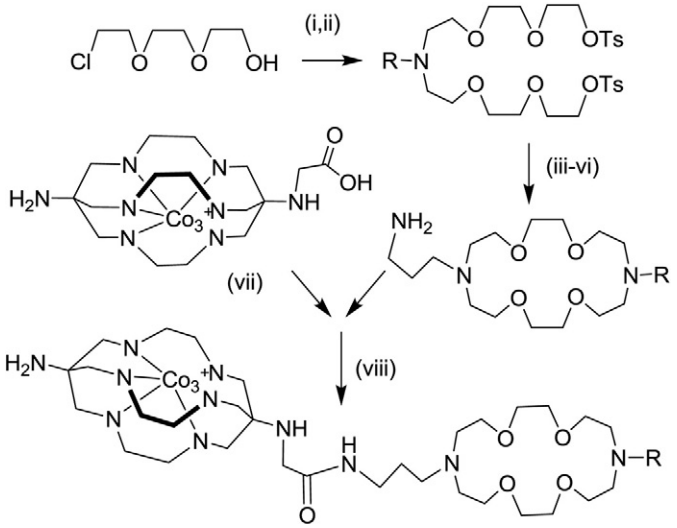

Scheme 2. Synthesis of cobalt cage amphiphile. (i) DMF, K_2CO_3, 4d; (ii) p-TsCl, NaOH/THF, 0 °C; (iii) $BzNH_2$, MeCN, Na_2CO_3, 3d; (iv) H_2, Pd/C 50 °C, 8 h; (v) CH_2CHCN, 12 h; (vi) = (iv), (vii) $SOCl_2$, 3 h; (viii) K_2HPO_4, RT, 12 h. **2**, R = $C_{16}H_{33}$; **3**, R = $C_{18}H_{37}$.

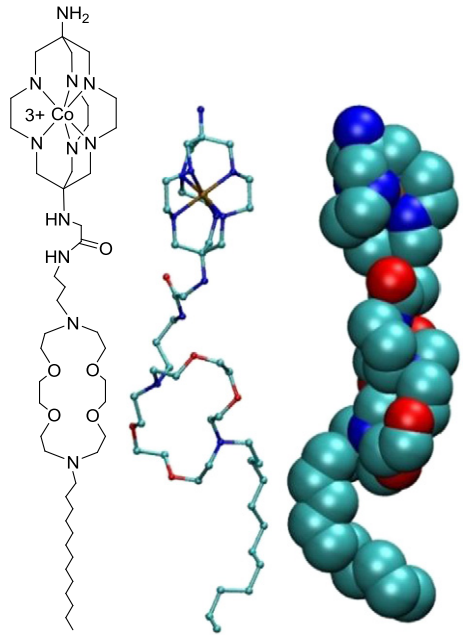

Fig. 1. Chemical and semi-empirical energy minimized structures of **1** (PM6 method [29]; COSMO [30] solvation; Mopac9 [29,31]).

and inverse micelles (>1). We utilize molecular modeling, surface tension measurements of the critical micelle concentration, and compared these estimates to atomic force microscopy previously reported [26] to test the PPM model for this class of novel surfactant.

A further geometrical consideration is that unimolecular **1**–**3** are unlikely to span the entire bilayer membrane in a manner which establishes a stable channel. We therefore posit that ion transport typical of channel formation can only originate through cooperative effects between monomers [8,9,32–37].

We conclude this report by interpreting the combined results according to the precepts of a toroidal pore model and hypothesize on the proximal interactions that are likely to establish such pores in the bilayer when **1**–**3** and their guest ions interact with the membrane.

2. Experimental section

2.1. Materials and methods

1,2-Diphytanoyl-sn-glycero-3-phosphocholine (DPhPC) and 1,2-dipalmitoyl-*sn*-glycero-3-phosphocholine (DPPC) were purchased

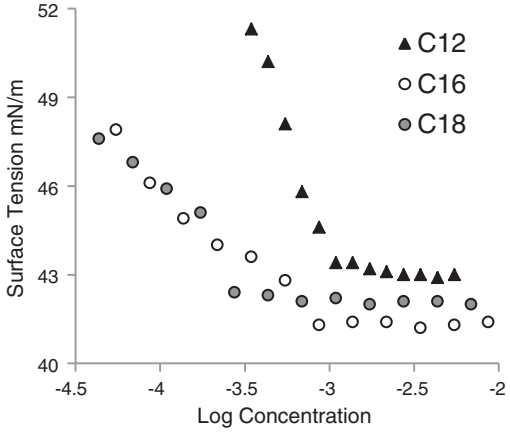

Fig. 2. Critical micelle concentration by discontinuity in surface tension for **1**–**3** (C_{12}, C_{16}, C_{18}).

from Avanti Polar Lipids (Alabaster, AL). KCl, $MgCl_2$, $CaCl_2$, pentane, decane, chloroform and N-(2-hydroxyethyl) piperazine-N-2-ethanesulphonic acid (HEPES) were purchased from Sigma-Aldrich (St. Louis, MO), and used without further purification. Deionized water was used in the preparation of all electrolyte solutions. Distilled chloroform was used to prepare lipid stock solutions. Nuclear magnetic resonance spectra were acquired using either a 300 MHz or 600 MHz Avance III BrukerUltrashield Spectrometer in $CDCl_3$, D_2O, or d_6-DMSO obtained from Sigma-Aldrich with TMS as the internal standard. Chemical shifts are reported in ppm (δ). Infrared spectra were recorded on a Perkin Elmer FT-IR Spectrum RX1 Spectrometer using KBr disks. Mass spectra were recorded on a Bruker ESI MicroTOFq. Compounds **1**–**3** were obtained from Richard A. Fairman and Gina E. Jaggernauth and prepared by substituting appropriate amines into Scheme 2 [26]:

Compound 2 ^{1}H NMR (D_2O, 400 MHz) δ: 0.80 (3H's), 1.2–1.9 (30H's), 2.4–4.2 (66H's); ^{13}C NMR (D_2O, 400 MHz) δ: 14.02, 22.74, 25.10, 26.62, 27.93, 29.58, 29.92, 30.03, 32.06, 43.33, 46.75, 47.03, 52.83, 57.51, 60.35, 61.61, 64.70, 67.91, 69.62, 71.74, 72.07; IR (neat) 1678 cm^{-1} (CONH); MS (ESI) *m/z* 1022 [$C_{47}H_{96}CoN_{11}O_5Na_3$].

Compound 3 ^{1}H NMR (D_2O, 400 MHz) δ: 0.82 (3H's), 1.2–2.0 (34H's), 2.8–4.2 (66H's); ^{13}C NMR (D_2O, 400 MHz) δ: 14.00, 22.72, 25.16, 27.85, 28.52, 30.08, 32.06, 43.10, 48.28, 48.77, 53.30, 57.44, 60.55, 55.55, 63.84, 69.46, 69.85, 70.95, 71.99; IR (neat) 1682 cm^{-1} (CONH); MS (ESI) *m/z* 1054.77 [$C_{49}H_{100}CoN_{11}O_5Na(CH_3OH)$].

2.2. Molecular modeling

Semi-empirical quantum mechanical calculations were done with the PM6 method in MOPAC [29,31] software, which is parameterized for closed-shell transition metals, by a three stage procedure. Firstly, a preliminary geometry optimization was performed using MOZYME [29,31] a localized molecular orbital alternative to SCF which shows rapid convergence for large protein-like molecules. The second calculation begins with the geometry obtained from the first, tightens the convergence criteria threshold, and computes the electrostatic interactions between the test compound and water molecules (ε=78.93, radius = 1.39 Å) to obtain the water-excluded dimensions (conductor like screening model, COSMO [30]). Third stage calculations involved reproducibility checks and establishing the variances obtained by changing, for example, the number of triangular segments per atom or the radius of the transition metal used in COSMO. Repeated runs in this manner were used to search the configuration space of geometries for **1**.

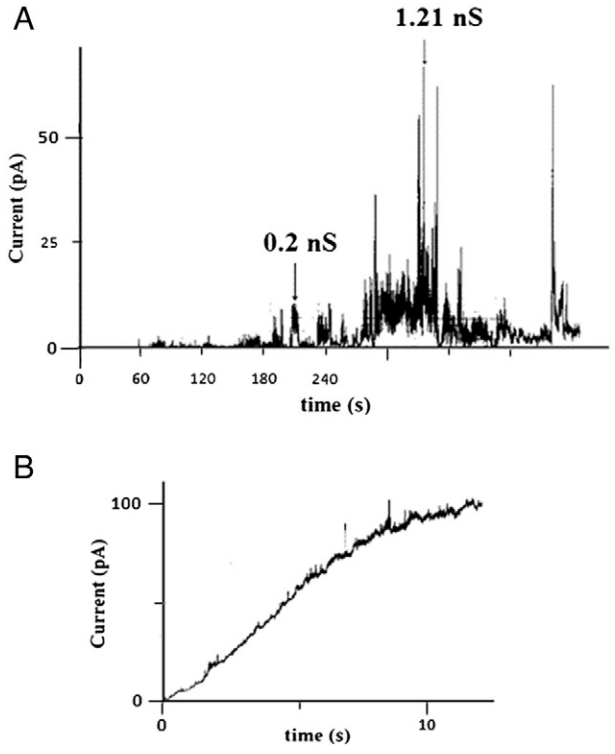

Fig. 3. (A) Erratic membrane activity of **1** in painted DPhPC membrane (15 μM in 1 M KCl at +60 mV potential). (B) Membrane carrier activity of **2** in painted DPhPC bilayers. (6 μM of **2** in 1 M $CaCl_2$ at +40 mV potential).

2.3. Planar lipid bilayer measurements

2.3.1. Painted bilayer membrane

Two compartments of a Teflon cell filled with 5 mL electrolyte solution were connected by a small circular aperture with a diameter of about 0.8 mm^2 [38]. The lipid membrane was formed by painting a 1% (w/v) DPhPC/decane solution across a precoated (usually a droplet of lipid immersed in pentane) hole using a Teflon coated metal loop. The quality of the bilayer membranes was checked by their stability under an applied potential for about 10–60 s time, as well as by observing the formation of the black planar lipid membrane through a monocular. Aliquots of concentrated stock solutions (**1**, 17.1 mM in methanol; **2** and **3**, 5 mM in methanol) were added to the electrolyte solutions on both sides of the bilayer membrane. Some control measurements were performed under single side addition but no asymmetry was observed. As for single side addition the equilibrium required longer time, we preferred both side addition. Ag/AgCl electrodes were connected to a voltage source and a current-to-voltage converter (Keithley 602, Gain: 10^9 V/A; rise time 30 ms) for the electrical measurements. The amplified signal was recorded with a strip chart recorder with about 0.1 s time resolution. In order to balance possible voltage-offset we zeroed the current at zero applied external voltage. All measurements have been done at room temperature (about 22–24 °C).

2.3.2. Solvent-free (also called folded or solvent-depleted) membrane

The lipid bilayer was prepared from a solution of DPhPC in pentane according to the technique of Montal and Mueller [39]. The membrane is formed across a 100–150 μm diameter hole (precoated with a droplet of hexadecane/pentane) in a 25 μm thick Teflon film clamped between Delrin half-cells. These half-cells were filled with approximately 2.8 mL of electrolyte solution, onto which 2–3 μL of DPhPC/pentane solution was applied. After evaporation of the pentane (~20 min) the electrolyte level in one half-cell was gently lowered and raised passed the hole, resulting in the folded membrane. The Delrin cell was enclosed in a double isolated Faraday cage and placed on a vibration isolating table. The quality of the bilayer membranes was checked by capacitance measurements, which was usually around 150 pF, and their stability under an applied potential for about 10–60 s. The apparatus was connected to the external circuit through a pair of homemade Ag/AgCl electrodes. The electrode on the *cis* side of the measuring cell was grounded whereas the other (on the *trans* side) was connected to the headstage of an Axopatch 200B amplifier (Axon Instruments, Foster City, CA) in the voltage clamp mode. Aliquots of concentrated stock solutions (**1**, 17.1 mM in methanol; **2** and **3**, 5 mM in methanol) were added to the electrolyte solutions on both sides of the bilayer membrane. The data acquisition was monitored by the pClamp10 software (Axon Instruments) and was filtered with the low pass Bessel filter of the amplifier at 2–5 kHz. All measurements have been done at room temperature (about 22–24 °C).

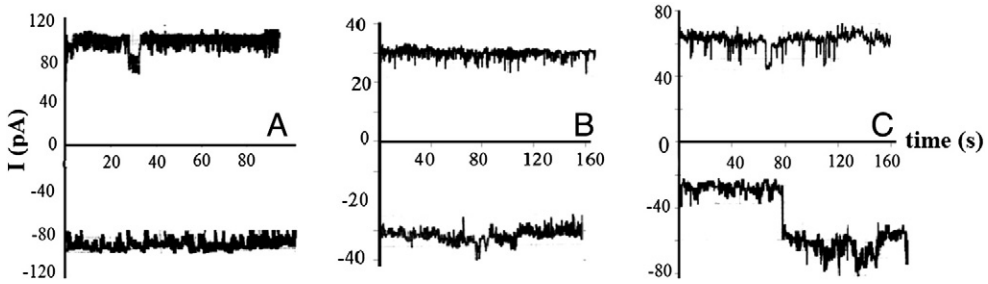

Fig. 4. Current profiles of long openings obtained for (A) 6 μM compound **3** in 1 M KCl at ± 40 mV, (B) 4 μM compound **3** in 1 M $CaCl_2$ at ± 60 mV and (C) 6 μM compound **3** in 1 M $MgCl_2$ at ± 40 mV, in solvent-free DPhPC membranes.

3. Results and discussion

3.1. Aggregation behavior and modeling

At a critical micelle concentration (cmc), most surfactant molecules are associated in densely packed groups whose interiors are hydrophobic and exteriors hydrophilic. With standard conditions of temperature and ionic strength, cmc values are inversely related to the ability of an amphiphile to affect surface tension. For compounds **1**–**3**, the corresponding cmc values by surface tension[2] (Fig. 2) are 1.1, 0.9 and 0.4 mM. These fall below binary cage-surfactants [22] (1.3 mM) and are a decade lower than a typical surfactant like SDS (8.3 mM). The trend is smaller than expected by Kleven's rule [33] relating logarithm of the cmc to aliphatic chain length in amphiphiles: Log (cmc) − b N_c, where b is a material constant and N_c is the number of carbon atoms in the tail, suggesting that the geometric PPM treatment may not fully apply for amphiphiles as diverse as **1**, and an incentive, thus, for molecular modeling.

We minimized the energy of several starting conformations of **1** using the semi-empirical PM6 quantum chemical method (which includes parameters for the transition metal) and the conductor-like screening model for solvent interactions (present in MOPAC9 [29,301]), yielding the lowest energy configuration shown in Fig. 1. The maximal dimensions are 29.7 × 10.6 × 9.5 Å and its solvent excluded volume is 1166.5 $Å^3$. From the height of compressed monolayers in the Langmuir isotherm experiment [26], the optimally-ordered hydrophobic groups in **1** are 19.5 Å long, in good agreement with the Tanford value [28] of 20.9 Å, but higher than the in-silico result (12 Å) where strong curvature of the tail appears in the free monomer. Turning to the head group, the mean molecular area of **1** is 153.5 $Å^2$, on par with a crown-free but double-tailed (154 $Å^2$) analog [34], but distant from a comparable single-tailed (85 $Å^2$) relative [35]. On its own, the aza-crown occupies only 22 $Å^2$ of monolayer interfacial area [36] while the area of the unsolvated cage is ≈80 $Å^2$ by crystallography [37] and 78 $Å^2$ from in-silico (herein) estimates. The remaining difference in area can be attributed to the high degree of solvation of the cage, with its counter ions, plus the area of the amide-linker oriented parallel rather than normal to the interface. Drawing on the model's solvent excluded volume now gives a packing parameter of 0.39, for which cylindrical micelles are the predicted and consistently observed aggregate structure [26].

3.2. Membrane activity

The membrane activity of **1**–**3** was evaluated by using the voltage clamp technique in two different planar bilayer systems and in the presence of different electrolytes. “Painted” or solvent-containing bilayers [27,38] were formed across the aperture of a Teflon barrier separating two symmetric salt solutions by painting the hole with a solution of the lipid (DPhPC) in decane. “Folded” (solvent-free) bilayers [27,39] were prepared through apposition of two lipid monolayers across the hole, achieved by steady lowering/raising the levels of electrolyte solution relative to the hole in the barrier. A comparison of the different techniques allows in elucidating the effects from their intrinsic difference in flexibility [27]. Subsequent to the formation of stable membranes, aliquots of compounds **1**–**3** in methanol were added to both sides of each membrane to yield the desired final concentrations. It is interesting to note that single sided addition yield similar results but required longer time for equilibrium. In each experiment, the stability and intrinsic conductance of the bilayer were also established using pure methanol as a control.

At low concentrations (<7.5 μM) and voltages between ± 60 mV and ± 100 mV, both types of bilayer membranes were unperturbed by compound **1**. The more fluid painted bilayers showed some activity at high concentrations (15 mM) or if the bilayer was doped with surfactant by breaking and reforming the membrane with **1** present in the electrolyte (Fig. 3A), but the conductive states are of high frequency and variable lifetimes.

These inhomogeneous and transient pores could not be improved by varying the concentration of **1** or the applied voltage across the membrane up to the membrane disruption limit [40,41]. Given the general susceptibility of DPhPC bilayer structures to changes in hydration [42], it is likely that the transient currents arise from random coincidences of increased curvature on opposed leaflets where the monomers of **1** are inserted [24,25,43,44]. However, there are few such spontaneous

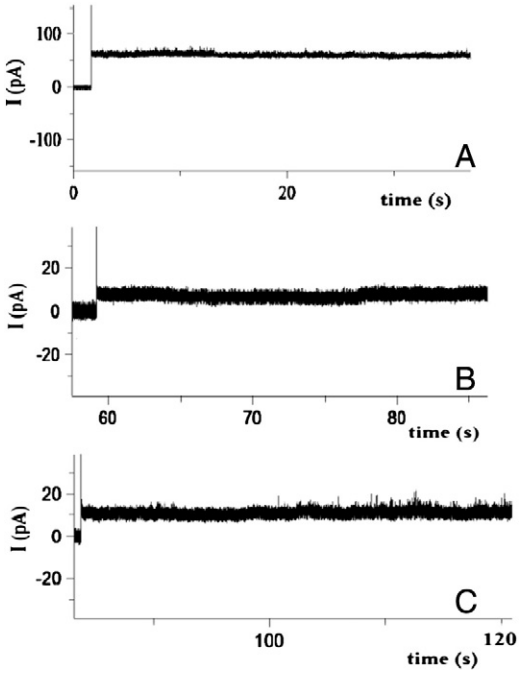

Fig. 5. Membrane activity of **2** in folded DPhPC bilayers with 6 μM of **2** in 1M (A) KCl, (B) $CaCl_2$ and (C) $MgCl_2$ at +40 mV potential.

[2] Supplementary data.

Table 1
Electrochemical properties of long-lived conducting pores formed by **2** in rigid bilayers and **3** in painted bilayers, with different electrolytes.

Surfactant	Electrolyte cation	Pore radius (nm)	Hill coefficient (n)	Specific conductance (nS/m)	Bulk conductance (S/m)
2	K	0.5	2.4	1.9	11.2
	Ca	0.2	2.3	0.4	11.6
	Mg	0.2	2.5	0.5	12.3
3	K	0.7	1.9	3.3	11.2
	Ca	0.5	1.6	2.4	11.6
	Mg	0.5	2.3	2.2	12.3

insertion sites as evidenced by the forcing conditions required to observe this activity.

Compound **2**, with the same C_{16} tail-group component as the DPhPC lipid, easily incorporated into both types of membrane. Even at low concentrations (2 μM) and applied voltage (±20 mV), concentration-dependent current fluxes were observed. The conductance was also easily restored after breaking and reforming the membrane, typical of compounds with high bilayer affinity. Notably, **2** produces the archetypical current profile of efficient carrier molecules [1,45] for several minutes of activity in the painted bilayer, with a steadily increasing current over time (Fig. 3B).

Amphiphile **3** also exhibited concentration dependent activity in the painted bilayer, but the current begins with initial erratic activity before settling to a long-lived steady state, bypassing the ion-transporter activity regime. Since conductance of the bilayer was not restored if the membrane was broken and reformed, the mode of incorporation and its activity on painted membranes are evidently different from that of **2**. However, the steady current profile is indicative of **3** forming long-lived conductive "pores" across the bilayer membrane [19,41,46] (Fig. 4). If the surfactant is easily accommodated within the bilayer to form pores, then the stability of such conducting pores may be expected to increase with the more rigid folded membrane structures.

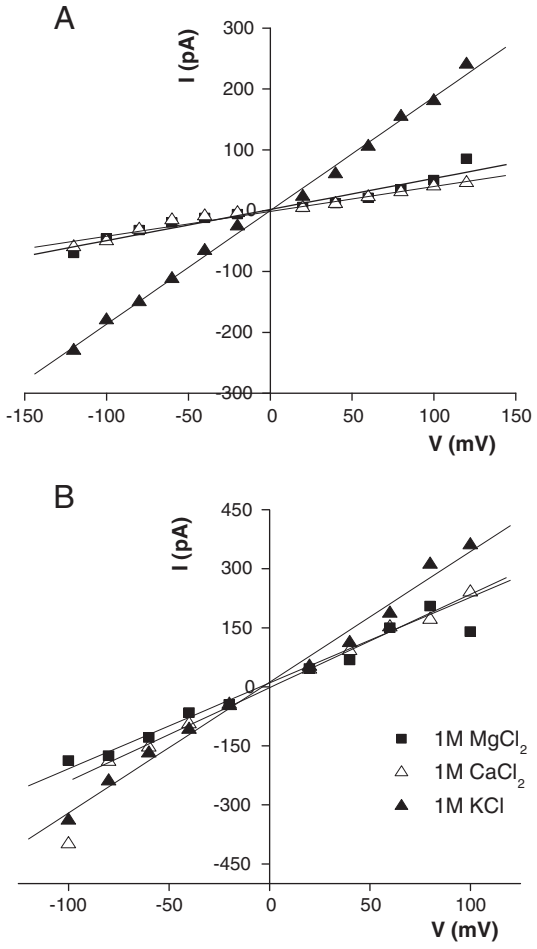

Fig. 6. Current–voltage plots in the presence of different electrolytes for (A) **2**, in a folded membrane and (B) **3**, in a painted membrane (6 μM of amphiphile).

The current profiles for **2** in folded bilayers are characterized by a short period of increasing current and an extended period of constant current, also attributable to the formation of long-lived pores (Fig. 5). The aza-crown substituent is expected to play an active solubilizing role in the transport of ions across the bilayer, whether as host transporter or through supramolecular assembly into membrane spanning pores. By comparing the average limiting currents with different cations (compensated for ionic activity) we may estimate this selectivity.

The average currents for **2** in folded bilayer membranes yield a selective order $K^+ > Mg^{2+} > Ca^{2+}$, opposing the trend in aqueous ionic conductivities for these ions (see Table 1). However, K^+ is also the largest of the group, and thereby most likely to adopt a sandwich-type coordination mode with the aza-crown ether [47,48] in the apolar interior of the bilayer. Observing that the trend is similar for **3** in the more fluid bilayer supports this hypothesis.

Surprisingly, **3** showed limited affinity for the rigid bilayer, and required similarly forcing conditions as **1** to establish moderate levels, though sporadic, of conductivity. In principle, the longer hydrophobic tail of **3** should enhance its incorporation into the membrane structure, but only the more fluid bilayer seems capable of easily accommodating the extra dimension (two methylenes) of the aliphatic tail in **3**. Also, evident in the conductivity profiles of **3** (Fig. 4C) is that more than one conductance level occurs (example at 80 s), indicative of either multiple species, with a different aggregation number, or that there is significant lateral diffusion of monomers within the bilayer leaflet which accelerates disaggregation [49]. With our results so far, we deem the former more likely, and seek to refine the aggregation-model of pore formation by examining the current–voltage relationships for each membrane (Fig. 6).

All the electrolyte solutions produce linear I–V plots, and the difference in the slope for K^+ activity in the rigid bilayer reinforces our earlier inference regarding the selectivity for K^+. From the slopes obtained, we can estimate the equivalent pore radius in each type of membrane system showing long-lived conducting states according to [1,41]:

$$G = \frac{\kappa \pi r^2}{l} \tag{1}$$

where G, the specific conductance, is the slope; κ is the bulk conductivity of the electrolyte; l is the thickness of the bilayer membrane and r the effective pore radius. Based on an assumed channel length of 3.4 nm [3], and taking into consideration the critical assumptions inherent in the application of Eq. 1 to the determination of the equivalent radius [1], we were thus able to approximate the radii of the membrane active structures, which are listed in Table 1.

With changing concentration of surfactant, the membrane conductance of **2** (Fig. 7A) and $\mathbf{3}^2$ increase non-linearly, suggesting a dynamic association/dissociation equilibrium [50] for the individual monomers which participate in the formation of active membrane pores.

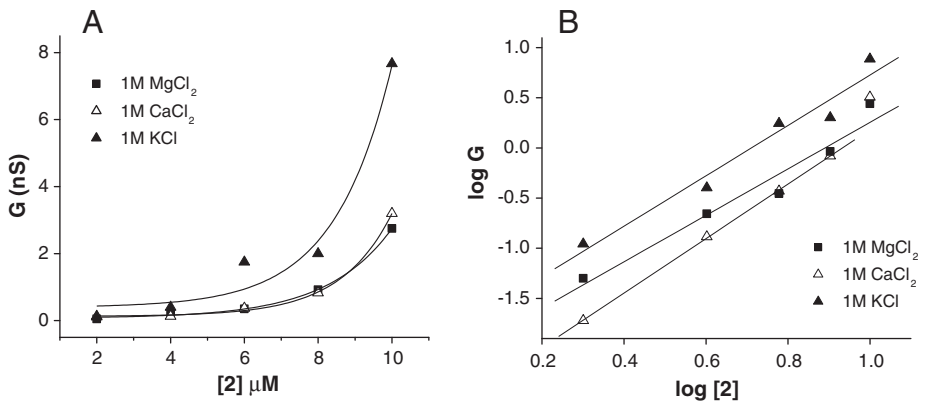

Fig. 7. (A) Membrane conductance, G, vs concentration of **2** in the presence of different electrolytes (+60 mV). (B) Hill plots for **2** in solvent-free membrane and the presence of different electrolytes.

According to the modified Hill equation [51], the conductance, G, is given by:

$$\log\ G = n\ \log\ C_M - n\ \log\ K_D \qquad (2)$$

where C_M is the monomer concentration, and n is the Hill coefficient, estimates the effective stoichiometry of the monomers in the active supramolecular species. The Hill plot for **2**with various electrolyte cations (Fig. 7B), and **3**†, are linear and yield the coefficients in Table 1. The more rigid bilayer is seen to conserve the effective supramolecular species in the conductive pore, while the more fluid bilayer gives larger variance in n values. In both cases, n averages to a value of 2, for which possible assembled configurations include a dimer, a tetramer (of two dimers) or similar even-numbered aggregates.

With the longer tailed C_{18}-amphiphile (**3**), higher effective pore radii and specific conductance are observed for the painted bilayer system, where the additional fluidity of the membrane is a necessary requirement for long-lived open states. In concert with the packing parameter analysis, this behavior is also reasonable: the longer tail reduces the cone angle subtended to the head group and increases compatibility with the bilayer, but limits the "free volume" which is available for water molecules to solubilize the guests (Scheme 3). Therefore, **3** is ineffective in the solvent-free bilayers but active in the painted bilayers.

The opposite situation applies for the shorter C_{12}-amphiphile, **1**, where the free volume is much larger but effective rigid-membrane penetration is limited by the higher cone angle.

3.3. Model of pore formation and membrane activity

We now discuss the membrane activity of **1**–**3** in relation to the labeled regions of the pictogram in Scheme 4.

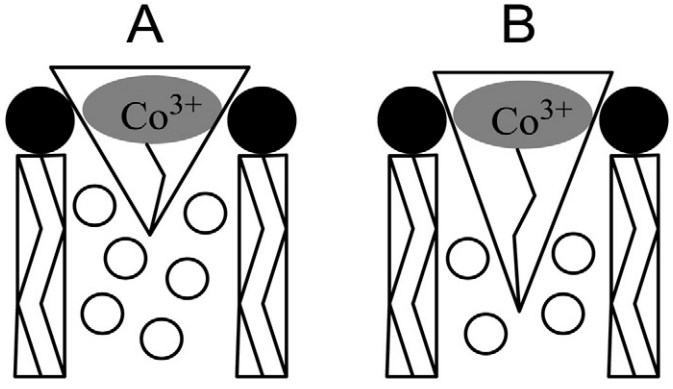

Scheme 3. Free volume (open circles) disparity between conical amphiphiles (A = short-tail, B = long-tail) and lipid bilayer.

The reported surface–pressure activity of **1** and its response to different guest cations in solution [26] supports the orientation of the cage group normal to the interface of polar/apolar membranes with the aza-macrocycle in a parallel orientation (A). The amide linker is very likely to be involved in binding a guest ion (B), as borne out by several studies of analogous functionalized diaza-crowns [52–54]. Such binding restricts, through electrostatic repulsion with the cage 3+ charge, the conformational space that is accessible to the headgroup (B). However, the guest cation becomes more lipid-soluble and its immersion into the bilayer also relieves the electrostatic and steric stress (C). Even singly, the partially incorporated surfactant will disrupt the interface, especially due to the high combined charges of the cage and guest [24,25]. In tandem, two amphiphiles with solubilized guest ions may induce even sharper membrane curvature (D) and begin the process of pore formation with the influx of requisite solvent and counterions for the charged groups. Large cations that are unable to fit on the interior of the macrocycle, and are instead "crowned" by one ring, may adopt the well-known sandwich-mode of coordination [47,48] between rings in search of thermodynamic stability through the macrocyclic effect [53]. If this occurs for two monomers in close proximity, the resultant merged-ring complex drives an even larger wedge into the bilayer (E). The extra cation is then released across the defect, giving rise to the bilayer current. With this formulation, the conductance lifetime is related to the affinity of the hydrophobic "anchors" (F) for the bilayer.

The pore assemblage process is consistent with the tail dimensions of **1**–**3**, which precludes direct membrane spanning pores; the Hill coefficient for the number of monomer units involved in the supramolecular transport process; the nonlinear current profiles with increased concentration of surfactant, which is indicative of an associative/dissociative equilibrium process regulating ion transport and even the erratic pore activity/detergent type membrane disruption at high concentrations of amphiphile.

The high values of the partition coefficients in binary liposome–amphiphile mixtures are indicative of strong compatible hydrophobic interactions, but are more likely dominated by a dipolar interaction between the highly charged cobalt-cage and the zwitterionic lipid headgroups. We may therefore also expect **1**–**3** to promote the type of membrane curvature described above leading to the formation of toroidal pores [24,44] spanning not a single leaflet, but the entire bilayer (Fig. 8).

4. Conclusions

In this study, we developed a novel class of synthetic ion transporters that induce transmembrane currents of various amplitudes depending on the nature of the membrane, the length of the alkyl chain and the guest ion interaction with the bridging macrocyclic cage. Semi-empirical quantum chemical calculations (PM6) on the

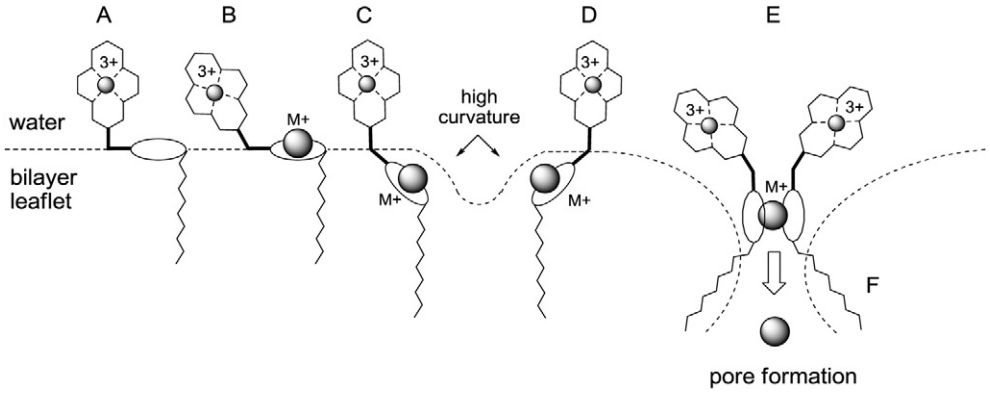

Scheme 4. Proposed mechanism and equilibria for the formation of long-lived conducting pores. The states labeled A–F are described in the text body.

minimum energy configurations for the first member of the series, **1**, generate excellent agreement between the predicted micellar structure and the cylindrical micelles observed by AFM on mica [26]. We have qualified the monomer self-assembly process in bilayers as a two component equilibrium process in which the high charge density of the aggregate headgroup induces strong curvature of the membrane, thereby initiating the formation of pores. We have also associated the stability of such pores with the strength of interaction between the hydrophobic regions of the amphiphile and the bilayer membrane through measures of the stability constants in binary liposomes and by DSC analysis of the membrane phase stability. We account for the fact that **1**–**3** do not show ion channel (distinct fluctuation between open and closed states) conductivity profiles with reference to the headgroup and crown orientation at the interfacial region which are too far apart to undergo stacking within the membrane.

Acknowledgement

The authors would like to thank The University of the West Indies, St. Augustine for providing a Graduate Student Research Award to Lorale J. Lalgee to undertake this research; and Jacobs University, Bremen, Germany for financial support.

Appendix A. Supplementary data

Supplementary data to this article can be found online at http://dx.doi.org/10.1016/j.bbamem.2014.01.032.

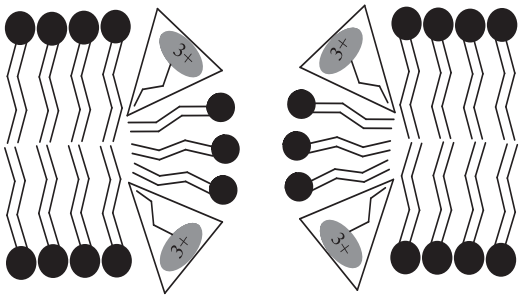

Fig. 8. Limiting "toroidal" pore formation by low concentrations of **2** and **3** in bilayer membranes.

References

[1] B. Hille, Ion Channels of Excitable Membranes, third ed. Sinauer Associates, Inc., Sunderland, MA, 2001.
[2] T.M. Fyles, Synthetic ion channels in bilayer membranes, Chem. Soc. Rev. 36 (2007) 335–347.
[3] S. Matile, A. Som, N. Sordé, Recent synthetic ion channels and pores, Tetrahedron 60 (2004) 6405–6435.
[4] S. Matile, A.V. Jentzsch, J. Montenegro, A. Fin, Recent synthetic transport systems, Chem. Soc. Rev. 40 (2011) 2453–2474.
[5] G.W. Gokel, M.M. Daschbach, Coordination and transport of alkali metal cations through phospholipid bilayer membranes by hydraphile channels, Coord. Chem. Rev. 252 (2008) 886–902.
[6] N. Madhavan, E.C. Robert, M.S.A. Gin, Highly active anion-selective aminocyclodextrin ion channel, Angew. Chem. Int. Ed. 44 (2005) 7584–7587.
[7] N. Yoshino, A. Satake, Y. Kobuke, An artificial ion channel formed by a macrocyclic resorcin[4]arene with amphiphilic cholic acid ether groups, Angew. Chem. Int. Ed. Engl. 40 (2001) 457–459.
[8] A.J. Wright, S.E. Matthews, W.B. Fischer, P.D. Beer, Novel resorcin[4]arenes as potassium-selective ion-channel and transporter mimics, Chem. Eur. J. 7 (2001) 3474–3481.
[9] V. Sidorov, F.W. Kotch, G. Abdrakhmanova, R. Mizani, J.C. Fettinger, J.T. Davis, Ion channel formation from a calix[4]arene amide that binds HCl, J. Am. Chem. Soc. 124 (2002) 2267–2278.
[10] N. Jayasuriya, S. Bosak, S.L. Regen, Design, synthesis, and activity of membrane-disrupting bolaphiles, J. Am. Chem. Soc. 112 (1990) 5844–5850.
[11] G.W. Gokel, I.A. Carasel, Biologically active, synthetic ion transporters, Chem. Soc. Rev. 36 (2007) 378–389.
[12] G. Das, P. Talukdar, S. Matile, Fluorometric detection of enzyme activity with synthetic supramolecular pores, Science 298 (2002) 1600–1602.
[13] N. Sordé, G. Das, S. Matile, Enzyme screening with synthetic multifunctional pores: focus on biopolymers, Proc. Natl. Acad. Sci. U. S. A. 100 (2003) 11964–11969.
[14] X. Li, B. Shen, X. Yao, D. Yang, Synthetic chloride channel regulates cell membrane potentials and voltage-gated calcium channels, J. Am. Chem. Soc. 131 (2009) 13676–13680.
[15] M. Tsikolia, A.C. Hall, C. Suarez, Z.O. Nylander, S.M. Wardlaw, M.E. Gibson, K.L. Valentine, L.N. Onyewadume, D.A. Ahove, M. Woodbury, M.M. Mongare, C.D. Hall, Z. Wang, B. Draghici, A.R. Katritzky, Synthesis and characterization of a redox-active ion channel supporting cation flux in lipid bilayers, Org. Biomol. Chem. 7 (2009) 3862–3870.
[16] E. Parera, F. Comelles, R. Barnadas, J. Suades, New surfactant phosphine ligands and platinum(II) metallosurfactants. influence of metal coordination on the critical micelle concentration and aggregation properties, Langmuir 26 (2010) 743–751.
[17] P.C. Griffiths, I.A. Fallis, T. Chuenpratoom, R. Watanesk, Metallosurfactants: interfaces and micelles, Adv. Colloid Interface Sci. 122 (2006) 107–117.
[18] D. Shukla, V.K. Tyagi, Cationic geminic surfactants: a review, J. Oleo Sci. 55 (2006) 381–390.
[19] L.M. Cameron, T.M. Fyles, C. Hu, Synthesis and membrane activity of a bis(metacyclophane) bolaamphiphile, J. Org. Chem. 67 (2002) 1548–1553.
[20] A.M. Sargeson, P.A. Lay, Dependence of the properties of cobalt(III) cage complex as a function of the derivatization of amine substituents, Aust. J. Chem. 62 (2009) 1280–1290.
[21] C. Behm, P.F.L. Boreham, I.I. Creaser, B. Korybut-Daszkiewicz, D.J. Maddalena, A.M. Sargeson, G.M. Snowdown, Novel cationic surfactants derived from metal ion cage complexes: potential antiparasitic agents, Aust. J. Chem. 48 (1995) 1009–1030.
[22] G.W. Walker, R.J. Geue, A.M. Sargeson, C.A. Behm, Surface-active cobalt cage complexes: synthesis, surface chemistry, biological activity, and redox properties, Dalton Trans. (2003) 2992–3001.
[23] A.M. Sargeson, The potential for the cage complexes in biology, Coord. Chem. Rev. 151 (1996) 89–114.
[24] H. Heerklotz, Interactions of surfactants with lipid membranes, Q. Rev. Biophys. 41 (2008) 205–264.

[25] H. Heerklotz, J. Seelig, Leakage and lysis of lipid membranes induced by the lipopeptide surfactin, Eur. Biophys. J. 36 (2007) 305–314.
[26] G. Jaggernauth, R.A. Fairman, Synthesis and characterization of an amphiphilic cobalt cage complex with aza-crown spacer, Inorg. Chem. Commun. 14 (2011) 79–82.
[27] P. Van Gelder, F. Dumas, M. Winterhalter, Understanding the function of bacterial outer membrane channels by reconstitution into black lipid membranes, Biophys. Chem. 85 (2000) 153–167.
[28] C. Tanford, The Hydrophobic Effect: Formation of Micelles and Biological Membranes, second ed. Wiley & Sons, New York, 1980. 39–45.
[29] J.J.P. Stewart, Optimization of parameters for semiempirical methods V: modification of NDDO approximations and application to 70 elements, J. Mol. Model. 13 (2007) 1173–1213.
[30] A. Klamt, The COSMO and COSMO-RS solvation models, WIREs Comput. Mol. Sci. 1 (2011) 699–709.
[31] J.J.P. Stewart, Computational Chemistry, http://OpenMOPAC.net (accessed 2008).
[32] T. Heimburg, Thermal Biophysics of Membranes, Wiley-VCH, Weinheim, Germany, 2007.
[33] H.B. Klevens, Structure and aggregation in dilate solution of surface active agents, J. Am. Oil Chem. Soc. 30 (1953) 74–80.
[34] E.J. Wanless, R.M. Pashley, Surface and aqueous solution properties of a highly charged cage surfactant, Colloids Surf. 56 (1991) 201–215.
[35] M.E. Karaman, R.M. Pashley, N.K. Bolonkin, Study of the surface and biological activity of a trivalent cage surfactant, Langmuir 11 (1995) 2872–2880.
[36] G.R.J.M. Klein, A.J. Sandee, F.G.A. Peters, S.J. van der Gaast, M.C. Feiters, R.J.M. Nolte, Aggregation of a crown ether-based copper amphiphile as a mimic for the superstructure of hemocyanin, J. Chem. Soc. Dalton Trans. 20 (2001) 3056–3064.
[37] R.J. Geue, T.W. Hambley, J.M. Harrowfield, A.M. Sargeson, M.R. Snow, Metal ion encapsulation: cobalt cages derived from polyamines, formaldehyde, and nitromethane, J. Am. Chem. Soc. 106 (1984) 5478–5488.
[38] P. Mueller, D.O. Rudin, H.T. Tien, W.C. Wescott, Methods for the formation of single bimolecular lipid membranes in aqueous solution, J. Phys. Chem. 67 (1963) 534–535.
[39] M. Montal, P. Mueller, Formation of bimolecular membranes from lipid monolayers and a study of their electrical properties, Proc. Natl. Acad. Sci. U. S. A. 69 (1972) 3555–3566.
[40] J.M. Moszynski, T.M. Fyles, Synthesis, transport activity, membrane localization, and dynamics of oligoester ion channels containing diphenylacetylene units, Org. Biomol. Chem. 8 (2010) 5139–5149.
[41] T.M. Fyles, C.C. Tong, Long-lived and highly conducting ion channels formed by lipophilic ethylenediaminepalladium(II) complexes, New J. Chem. 31 (2007) 655–661.
[42] C.-H. Hsieh, S.-C. Sue, P.-C. Lyu, W.-G. Wu, Membrane packing geometry of diphytanoylphosphatidylcholine is highly sensitive to hydration: phospholipid polymorphism induced by molecular rearrangement in the headgroup region, Biophys. J. 73 (1997) 870–877.
[43] J. Verdon, M. Falge, E. Maier, H. Bruhn, M. Steinert, C. Faber, R. Benz, Y. Héchard, Detergent-like activity and α-helical structure of Warnericin RK, an anti-legionella peptide, Biophys. J. 97 (2009) 1933–1940.
[44] B. Bechinger, K. Lohner, Detergent-like actions of linear amphipathic cationic antimicrobial peptides, Biochim. Biophys. Acta 1758 (2006) 1529–1539.
[45] R. Benz, G. Stark, H. Jank, P. Läuger, Valinomycin-mediated ion transport through neutral lipid membranes: influence of hydrocarbon chain length and temperature, J. Membr. Biol. 14 (1973) 339–364.
[46] L. Ma, M. Melegari, M. Colombini, J.T. Davis, Large and stable transmembrane pores from guanosine–bile acid conjugates, J. Am. Chem. Soc. 130 (2008) 2938–2939.
[47] P. Comba, W. Schiek, Fit and misfit between ligands and metal ions, Coord. Chem. Rev. 238–239 (2003) 21–29.
[48] J.W. Steed, D.R. Turner, K.J. Wallace, Core Concepts in Supramolecular Chemistry and Nanochemistry, Wiley & Sons, Ltd., England, 2007. 39–45.
[49] C. Goto, M. Yamamura, A. Satake, Y. Kobuke, Artificial ion channels showing rectified current behavior, J. Am. Chem. Soc. 123 (2001) 12152–12159.
[50] R. Benz, A. Schmid, W. Wagner, W. Goebel, Pore formation by the *Escherichia coli* hemolysin: evidence for an association–dissociation equilibrium of the pore-forming aggregates, Infect. Immun. 57 (1989) 887–895.
[51] S. Litvinchuk, G. Bollot, J. Mareda, A. Som, D. Ronan, M.R. Shah, P. Perrottet, N. Sakai, S. Matile, Thermodynamic and kinetic stability of synthetic multifunctional rigid-rod β-barrel pores: evidence for supramolecular catalysis, J. Am. Chem. Soc. 126 (2004) 10067–10075.
[52] V.J. Gatto, K.A. Arnold, A.M. Viscariello, S.R. Miller, C.R. Morgan, G.W. Gokel, Syntheses and binding properties of bibrachial lariat ethers (BiBLEs): survey of synthetic methods and cation selectivities, J. Org. Chem. 51 (1986) 5373–5384.
[53] K. Suzuki, K. Watanabe, Y. Matsumoto, M. Kobayashi, S. Sato, D. Siswanta, H. Hisamoto, Design and synthesis of calcium and magnesium ionophores based on double-armed diazacrown ether compounds and their application to an ion sensing component for an ion-selective electrode, Anal. Chem. 67 (1995) 324–334.
[54] R.D. Hancock, A.E. Martell, Chelate ring geometry, and the metal ion selectivity of macrocyclic ligands. Some recent developments, Supramol. Chem. 6 (1996) 401–407.